ELSEVIER

Surface Science 418 (1998) 295–302

surface science

Domain-wall interactions in Bi/Cu(001)

H.L. Meyerheim [a,*], M. De Santis [b], W. Moritz [a], I.K. Robinson [c]

[a] *Institut für Kristallographie and Angew. Mineralogie, LMU München, Theresienstr. 41, D-80333 Munich, Germany*
[b] *Laboratoire de Cristallographie, CNRS, BP 166 F-38042 Grenoble cedex 9, France*
[c] *Department of Physics, University of Illinois, Urbana, IL 61801, USA*

Received 14 July 1998; accepted for publication 7 September 1998

Abstract

Surface X-ray diffraction has been used to determine the two-dimensional structures of Bi adsorbed on Cu(100) at coverages of 0.56 and 0.60 monolayers. At the lower coverage, a c($9\sqrt{2}\times\sqrt{2}$)R45 domain wall structure is formed consisting of a uniaxial dislocation array with a single row of Bi atoms inserted per unit cell. The p(10×10) structure at 0.6-monolayer coverage is a two-dimensional array of similar dislocations. This system presents a unique opportunity to observe the structure of the vertex formed when two dislocations cross and interact with each other. The mechanism of the interaction is revealed by analyzing the individual displacements of the atoms from their ideal lattice sites in both structures.

Keywords: Bismuth; Copper; Low index single crystal surfaces; Surface structure

1. Introduction

The structure and morphology of the first adsorbate monolayer on a crystal surface is one of the most important factors determining the properties of the growing interface. Consequently, the study of the interface formation in the monolayer range is of central interest in surface science. In this context, unreconstructed (001), (110) and (111) surfaces of fcc-metals serve as prototype substrates due to their simple geometrical structure. In general, the structures of close-packed monolayers on these surfaces can be roughly classified into two extreme cases, depending on the relative strength of the adatom–adatom (AA) and the adatom–substrate (AS) interaction. If the AA-interaction predominates over the AS-interaction (quasi-) hexagonal arrangements of the adatoms are found. For example, this model is well known for weakly bonded adsorbates like noble gases [1,2] or some large adatoms like Cs [3]. If the AS-interaction is stronger, the adatoms will be locked in special sites. If there is a size mismatch between the adsorbate and substrate atoms, the strain in the adsorbate layer may be released by the formation of regular misfit dislocations leading to large superstructure unit cells.

Just like their bulk analogues, surface dislocations are a common form of defect that can interrupt the long-range periodicity of a surface. They occur whenever there is sufficient misfit between one layer and its neighbor, notably in the case of adsorbed monolayers. According to the Frank van der Merwe model [4–7] analyzed theoretically by Pokrovski and Talapov [8], a regular

* Corresponding author. Fax: +49 89 2394 4334; e-mail: holger.meyerheim@lrz.uni-muenchen.de

0039-6028/98/$ – see front matter
PII: S0039-6028(98)00725-0

linear array of dislocations is the lowest energy state of a monolayer with a different natural spacing from the substrate. Surface dislocations are also spontaneously excited in otherwise perfect monolayers at sufficiently high temperatures and eventually lead to surface phase transitions. The structural properties of surface dislocations are therefore of great importance. Once arranged in regular arrays, these can be investigated by powerful crystallographic methods, such as X-ray diffraction. For linear arrays, this has been carried out for a number of systems [9,10]. The general result is that the adsorbate monolayer atoms reside in lattice sites if they are far away from the dislocation but are displaced close to the dislocation, i.e. within one or two atomic spacings. These findings are generally consistent with the principles of continuum elasticity. While detailed questions remain concerning the exact pattern of displacements in each individual system, just as in the pattern of layer spacings associated with surface relaxation, the next important general question to ask concerns the interactions between the dislocations on a surface: What is the nature of the vertices formed where dislocations meet? To answer this question, it is necessary to analyze the structure of a system, which forms a regular two-dimensional dislocation array. Here, we report that Bi/Cu(100), under appropriate coverage conditions, is such a system. The surprising result is that the vertices retain fourfold rotational symmetry, but break their mirror symmetry. The dislocations meet in a "pinwheel" arrangement with an offset of one unit cell spacing between the incoming dislocations on either side.

Previous experiments on the Bi/Cu(001) system have reported two superstructures for nearly dense and dense Bi-monolayers on Cu(001) [11,12], but no detailed structure analysis has been performed so far. On the basis of a geometric interpretation of low-energy electron diffraction (LEED) patterns, the phases formed at 0.56 and 0.60 monolayers (ML) coverage were designated as a c $(9\sqrt{2}\times\sqrt{2})$R45 and a $(\sqrt{41}\times\sqrt{41})$-R $\tan^{-1}$ (5/4) superstructure. We define 1 ML as a coverage of 1.53×10^{15} Bi atoms cm^{-2}, i.e. as 1 adatom per substrate (1×1) unit cell. In the following, we present in detail the results of the structure analyses where the second phase forming at 0.60 ML is correctly described as a $p(10\times10)$ superstructure, which is characterized by a two-dimensional array of dislocation lines.

2. Experimental results

The X-ray experiments were performed using an 18-kW rotating anode X-ray generator and a sagittally focusing pyrolytic graphite monochromator selecting CuKα radiation. The Cu(001) crystal ($Ø\approx10$ mm) was cleaned by standard procedures until no traces of contaminants were detectable by Auger electron spectroscopy (AES). Highly purified Bi (6 N) was deposited at an initial rate of 0.05 ML min^{-1} from a water-cooled Knudsen cell placed about 15 cm from the sample. In our previous study on the room-temperature (RT) low-coverage alloy formation, we discussed in detail the AES calibration of the different structures [13], which is not repeated here. After a deposition time of about 11 min, a clear two-domain $c(9\sqrt{2}\times\sqrt{2})$R45-LEED pattern is observed. In addition, the slope of the AES signals as a fuction of the Bi-deposition time decreases, which can be attributed to a change in the sticking probablility of the close-packed layer. After 24 min, the diffraction pattern looks similar to that described in fig. 2a of Ref. [11]. At this coverage, the positions of the reflections were found to correspond exactly to a $p(10\times10)$-superlattice cell.

For the $c(9\sqrt{2}\times\sqrt{2})$R45-superstructure, a total of 305 reflections were measured, reducing to 134 independent reflections by symmetry. In the case of the $p(10\times10)$ structure, 146 reflections were measured, reducing to 114 by symmetry equivalence. The reproducibility of the equivalent reflections is generally in the range between 6 and 10%, based on $|F|$. Fig. 1a shows superlattice and crystal truncation rods (CTR) for the $p(10\times10)$ structure. Each data point represents a structure factor amplitude, $|F|$, derived from an integrated intensity after correction for active sample area, Lorentz- and polarization factors [14,15]. Along the rods, a maximum momentum transfer, q_z, of two recip-

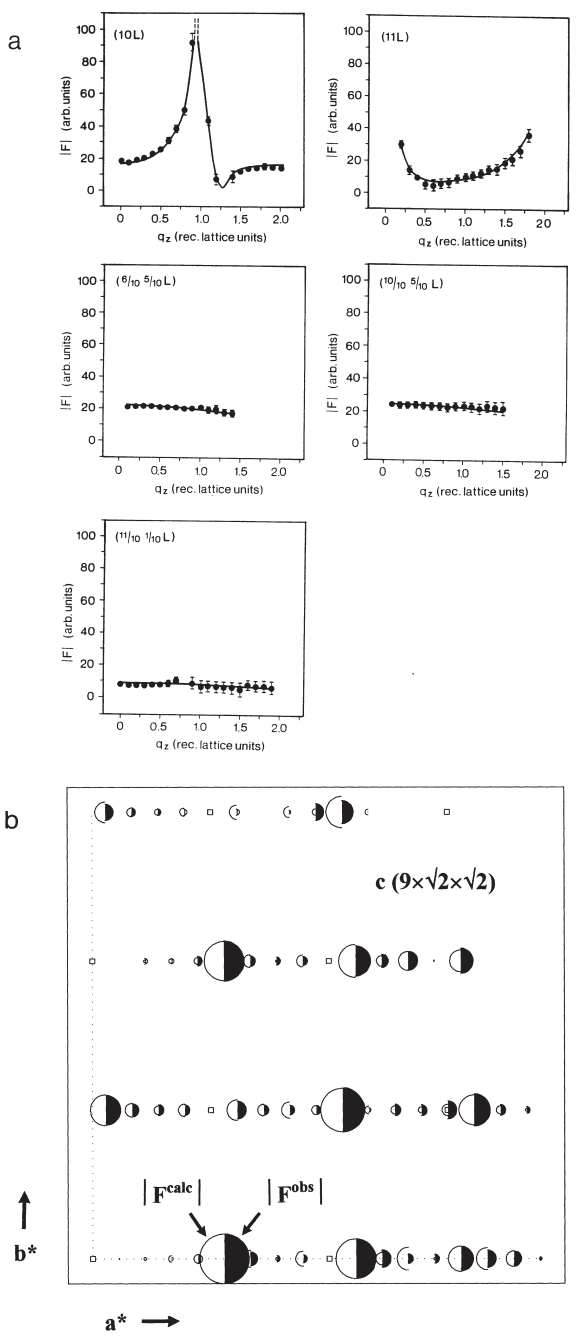

Fig. 1. (a) Measured (symbols) and calculated (lines) structure factor amplitudes along several superlattice and crystal truncation rods for Bi/Cu(001)-p(10×10). (b) In-plane (hk0) reflections for the c(9√2×√2)-structure. The radii of the open (calculated) and filled (measured) circles are proportional to the structure factor amplitudes, and their areas are proportional to the intensities.

rocal lattice units (rlu) corresponding to 3.48 $Å^{-1}$ could be achieved. The solid lines represent the best fit to the data according to the structure model discussed below. A similar fit quality is also obtained for the $c(9\sqrt{2}\times\sqrt{2})$R45-superstructure, and Fig. 1b shows the (hk0) reflections, where the radii of the open and filled semicircles represent the calculated and measured structure factors. For the complete data sets, we derive unweighted residua of $R_u = 12.6$ and 7.4% for the $c(9\sqrt{2}\times\sqrt{2})$R45 and the $p(10\times10)$ structure, respectively. The unweighted residuum is defined as:

$$R_u = \sum_{hkl} ||F_{hkl}^{obs}| - |F_{hkl}^{calc}|| / \sum_{hkl} |F_{hkl}^{obs}|.$$

2.1. *Bi/Cu(001)-c(9√2×√2)R45*

Fig. 2 shows top and side views of the structure. (We use a setting of the superstructure unit cell based on the primitive (p) (1×1) unit cell of the Cu(001) surface. This is related to the face (f) centered setting by $[100]_p = 0.5\cdot\{[100]_f + [010]_f\}$, $[010]_p = 0.5\cdot\{[100]_f - [010]_f\}$, and $[001]_p = [001]_f$). Large circles represent Bi-atoms, and small circles represent Cu-atoms, where the top-layer Cu-atoms are shown shaded. The atoms within the asymmetric unit of the superlattice cell (plane group cmm2) are labeled according to Table 1. In this structure model, the Bi coverage is 0.56 ML, and the refinement gave no evidence for defect sites within the Bi-layer. The right part of the figure indicates the interatomic distances between the symmetry-independent Bi-atoms. The arrows indicate the lateral shifts of the Bi-atoms from the positions, which would correspond to the unrelaxed $(\sqrt{2}\times\sqrt{2})$R45-structure. These are largest (0.52 Å) close to the domain boundary but rapidly damp out further away from the boundary. In addition to the lateral relaxations, the Bi-layer exhibits a height modulation of 0.50 (15) Å. This is shown in the side view of the structure. As a result of the relaxations, the Bi–Bi distances are almost equidistant. They are in the range between 3.28 (10) and 3.44 (10) Å, which is in between the shortest

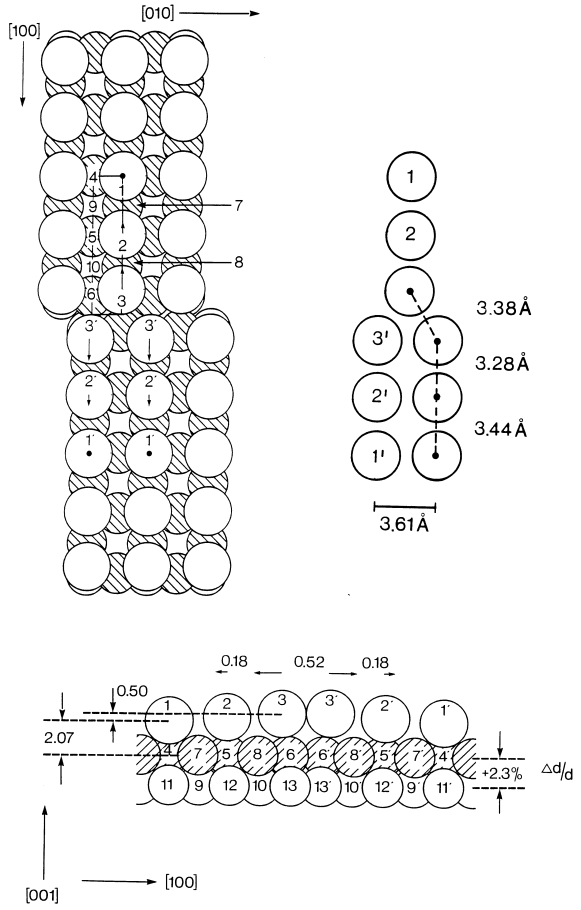

Fig. 2. (a) Schematic view of the c($9\sqrt{2}\times\sqrt{2}$)R45 structure. Large and small circles represent Bi and Cu atoms, respectively. First-layer Cu atoms are shown shaded. The atoms within the asymmetric unit are labeled according to Table 1, the Bi-atom shifts are indicated by the arrows, and their magnitudes are given in angstroms. Atoms labeled by primed numbers are symmetry related to the unprimed ones by the glide line at the antiphase boundary. The right part indicates the Bi-interatomic distances within the asymmetric unit. (b) Side view of the structure.

interatomic Bi-distances in the rhombohedral bulk structure (3.10 and 3.47 Å) [16,17].

The large relaxations in the Bi-layer at the domain boundaries are indicative of compressive strain in the Bi-layer, and a corresponding strain in the Cu-layer can be expected. We derive a lateral shift of 0.13 and 0.11 Å for the top-layer Cu atoms directly beneath the Bi-atoms at the antiphase boundary. Other Cu-atoms are shifted as well, but these relaxations are less important (0.04–0.07 Å) and within the error bar of the distance determination, which is about 0.10–0.15 Å. A vertical strain seems also plausible but could not be considered in detail in the analysis due to the limited resolution. Nevertheless, for the first-layer Cu atoms, we observe enhanced thermal (Debye) parameters, B, which are in the range between 2.6 and 6.1 Å^2. We suggest that this might compensate for neglecting a slight buckling of the first Cu layer, which, in the refinement, was assumed to be planar in order to reduce the number of refined parameters. For the Bi-atoms, we did not find any significantly enlarged B-factors ($B=0.6$ Å^2). The shortest Bi–Cu distances are in the range between 2.70 and 2.80 Å, which corresponds to an effective hard sphere Bi-radius of 1.43–1.53 Å, compatible with the shortest bulk interatomic Bi-distance. Finally, the lateral Cu-relaxations are accompanied by a 2.3% expansion of the first Cu-interlayer spacing, in such a way as to keep the Cu-interatomic distances of the second layer within a range below 3% of the bulk distance (2.556 Å).

Our results compare quite well with the similar Pb/Cu(001) c($5\sqrt{2}\times\sqrt{2}$)R45 structure analyzed with LEED [9]. In this case, the Pb atoms at the domain boundaries are shifted 0.40 (10) Å out of the hollow sites, and the first interlayer distance was also found to expand by (at most) 1–2%, but only a small Pb corrugation of 0.05 Å was determined.

2.2. *Bi/Cu(001)-p(10×10)*

Fig. 3a shows a top view of one unit cell (plane group p4gm) of the p(10×10) structure. The solid triangle indicates the asymmetric unit in which the Bi-atoms are labeled according to Table 2. The arrows and the small numbers refer to the Bi-shifts in units of 1/100 Å. Basically, the p(10×10) structure can be considered as a two-dimensional extension of the $c(9\sqrt{2}\times\sqrt{2})$R45-structure with the dislocation lines running along two mutually orthogonal ⟨100⟩ directions of the substrate. The dislocation lines intersect at the fourfold symmetry axes where the lateral Bi-relaxations are larger [max. 0.63(7) Å] than in the case of the $c(9\sqrt{2}\times\sqrt{2})$R45-structure, because of the larger

Table 1
Structure parameters for of the final model of the c($9\sqrt{2}\times\sqrt{2}$)R45-structure

Atom	x	y[a]	z[b]	B (Å^2)	$\Delta(x)$ (Å)[c]
# 1 Bi	0.000	$\frac{1}{2}$	1.57[a]	0.60[a]	0.00
# 2 Bi	0.106 (1)	$\frac{1}{2}$	1.62[a]	0.60[a]	0.18
# 3 Bi	0.206 (1)	$\frac{1}{2}$	1.71[a]	0.60[a]	0.52
# 4 Cu	0.000	0	1.00	0.60[a]	0.00
# 5 Cu	0.110 (1)	0	1.00	3.4 (1.7)	0.04
# 6 Cu	0.219 (2)	0	1.00	3.7 (1.8)	0.11
# 7 Cu	0.053 (1)	$\frac{1}{2}$	1.00	6.1 (2.1)	0.07
# 8 Cu	0.163 (1)	$\frac{1}{2}$	1.00	2.6 (1.7)	0.13
# 9 Cu	0.054 (1)	0	0.49	0.6[a]	0.04
# 10 Cu	0.167 (1)	0	0.49	0.6[a]	0.00
# 11 Cu	0.000[a]	$\frac{1}{2}$	0.49	0.6[a]	0.00
# 12 Cu	0.111[a]	$\frac{1}{2}$	0.49	2.8 (1.3)	0.00
# 13 Cu	0.222[a]	$\frac{1}{2}$	0.49	0.6[a]	0.00

Lattice constants: $a_0=32.54$ Å, $b_0=3.61$ Å, $c_0=3.61$ Å
Non-structural parameters: two scale factors, roughness factor $\beta=0.07$
134 reflections: $R_u=0.12$
Distances (Å) (error $\approx$ 0.10 Å):
1Bi–2Bi: 3.44 1Bi–4Cu: 2.75 1Bi–7Cu: 2.70
2Bi–3Bi: 3.28 2Bi–7Cu: 2.82 2Bi–5Cu: 2.88 2Bi–8Cu: 2.90
3Bi–3′Bi: 3.38[d] 3Bi–8Cu: 2.93 3Bi–6Cu: 3.17
4Cu–7Cu: 2.50 4Cu–9Cu: 2.56
5Cu–7Cu: 2.59 5Cu–8Cu: 2.49 5Cu–9Cu: 2.59 5Cu–10Cu: 2.51
6Cu–8Cu: 2.57 6Cu–10Cu: 2.51
7Cu–11Cu: 2.51 7Cu–12Cu: 2.61
Covalent radii: Bi: 1.82 Å; Cu: 1.28 Å
Distances in bulk structures: Bi: 3.09 Å, 3.47 Å; Cu: 2.56 Å

The atom positions are given in relative coordinates of the unit cell. For the modeling of the disorder, we used the isotropic Debye parameter (B) defined as $B=8\pi^2\langle u^2\rangle$, where $\langle u^2\rangle$ is the mean squared displacement.
[a]Not refined parameter.
[b]Third Cu-layer at $z=0.0$
[c]Displacements relative to ideal ($\sqrt{2}\times\sqrt{2}$)R45-positions.
[d]Distance to symmetry equivalent Bi in the adjacent domain (labeled by prime).

strain imposed on the Bi-overlayer at these positions. This has no notable influence on the amplitude of the vertical buckling of the Bi-layer, which is 0.42 (15) Å. Due to the dominant Bi-contribution, and the smaller data set in the present case, we did not include any lateral Cu-relaxations, but we allowed the (planar) first Cu layer to relax vertically ($\Delta d/d=+4\%$) and refined an overall B-factor ($B=1.6$). The interlayer expansion is larger than that found in the $c(9\sqrt{2}\times\sqrt{2})$R45-structure and might be somewhat overestimated because of neglecting some layer buckling as well as vertical disorder. The shortest interatomic Bi–Cu distances are generally in the range between 2.69 (15) and 2.90 (15) Å. There is only one shorter distance (2.64 Å) but this depends critically on the lateral shift of the #4 Bi atom and the Cu-relaxation. These results translate to an effective Bi-radius in the range between 1.42 and 1.63 Å, i.e. there is no notable change as compared to the $c(9\sqrt{2}\times\sqrt{2})$ R45-structure. This also applies to the Bi–Bi distances, which do not deviate more than 4–7% from the average value of 3.29 Å.

3. Discussion

Clearly, both structures can be classified as domain wall structures interrupting otherwise

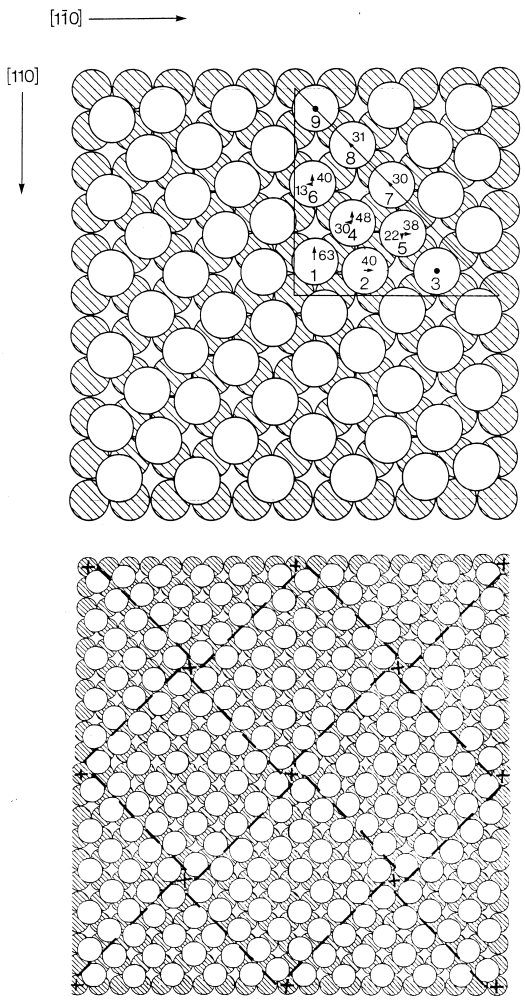

Fig. 3. (a) Schematic view of one $p(10\times10)$ unit cell. The solid triangle indicates the asymmetric unit. The small numbers refer to the shifts in 1/100 angstrom units. The atoms are labeled according to Table 2. (b) Plot of four $p(10\times10)$ superstructure cells showing the clockwise and anticlockwise arrangement of the domains. The domain boundaries are indicated by the dashed lines.

$(\sqrt{2}\times\sqrt{2})$ arrays of Bi atoms residing in hollow sites. In both cases, the domain walls are of the "heavy" type since the average density of Bi atoms exceeds the primitive state corresponding to $\theta_{Bi}=0.5$ ML, where one Bi-adatom occupies one $(\sqrt{2}\times\sqrt{2})$ surface unit cell; along the core of the surface dislocation represented by the domain wall, Bi atoms occupy adjacent hollow sites in the Cu substrate. The principal difference between the two structures is that the $c(9\sqrt{2}\times\sqrt{2})$ structure, is a one-dimensional (uniaxial) domain-wall structure, whereas the $p(10\times10)$ is a two-dimensional array. Each unit cell of the $p(10\times10)$ also contains two vertices where the surface dislocations cross each other. The vertices sit on fourfold axes of the p4 structure, but notably do not possess a 4mm symmetry. The dislocations meet in an offset manner to create "pinwheel" structures, spiraling alternately clockwise and counter-clockwise. This can be seen in Fig. 3b, where several $p(10\times10)$ unit cells are plotted, and the domain boundaries are indicated by dashed lines. The lower-symmetry arrangement presumably provides an energetically more favorable structure than the higher-symmetry arrangement because it allows more possibilities for relaxation. In between the crossing dislocation lines lie rectangular 3×4 islands of the $(\sqrt{2}\times\sqrt{2})$ -Bi structure, zigzagging in the x- and y-directions.

Our crystallographic refinement provides the individual displacements of each atom from the ideal lattice sites, which allows a posteriori analysis of the distribution of strain. Direct comparison of the $c(9\sqrt{2}\times\sqrt{2})$-structure with the $p(10\times10)$ allows detection of the differences in strain relaxation when the second dimension can be exploited. Within the islands of the $c(9\sqrt{2}\times\sqrt{2})$-structure, the Bi–Bi interatomic spacings are contracted to 3.44 and 3.28 Å from the 3.615 Å $(\sqrt{2}\times\sqrt{2})$ spacing, which is quite significant when compared with an error bar of 0.05–0.10 Å. The contraction is along a single axis because of the constraints of symmetry. Within the dislocation itself, the Bi–Bi spacing is 3.38 Å (distance between atoms labeled 3 and 3′ in Fig. 2). The Bi atoms within the dislocation have five neighbors in-plane instead of four for the $(\sqrt{2}\times\sqrt{2})$ regions, but the contacts to the Cu substrate are correspondingly disrupted by the displacements. Thus, in the positions where symmetry allows relaxation, the Bi adopts a Bi nearest-neighbor spacing that approaches that of bulk Bi, which is 3.29 Å on average.

The domain walls of the $p(10\times10)$ structure are allowed to relax in addition along the dislocation axis, and the diagonal Bi–Bi distance (i.e. the distances across the dislocation line) is found to

Table 2
Structure parameters for of the final model of the p(10 × 10)-structure

Atom	x	y	z	B (Å^2)	$\Delta(x)$ (Å)[a]	$\Delta(y)$ (Å)[a]
# 1 Bi	0.051 (3)	0.074 (3)	1.19 (3)	1.6 (3)[b]	0.02	0.63
# 2 Bi	0.166 (3)	0.053 (3)	1.15 (3)	1.6 (3)	0.40	0.07
# 3 Bi	0.350[e]	0.050[e]	1.07[d]	1.6 (3)	0.00	0.00
# 4 Bi	0.138 (3)	0.169 (4)	1.16[d]	1.6 (3)	−0.30	0.48
# 5 Bi	0.265 (3)	0.141 (4)	1.16[d]	1.6 (3)	0.38	−0.22
# 6 Bi	0.045 (3)	0.266	1.14[d]	1.6 (3)	−0.13	0.40
# 7 Bi	0.238 (3)	0.262[e]	1.16[d]	1.6 (3)	−0.30	0.30
# 8 Bi	0.137 (3)	0.363[e]	1.16[d]	1.6 (3)	−0.32	0.30
# 9 Bi	0.050 (3)	0.450[e]	1.16[d]	1.6 (3)	0.00	0.00
# 10 Cu	0.000[e,f]	0.000[e,f]	0.52 (1)	1.6 (3)	First-layer Cu[f]	
# 11 Cu	0.050[e,f]	0.050[e,f]	0.00[e]	0.6[e]	Second-layer Cu[f]	

Lattice constants: $a_0 = 25.57$ Å, $b_0 = 25.57$ Å, $c_0 = 3.61$ Å
Non-structural parameters: two scale factors, roughness factor $\beta = 0.06$
114 reflections: $R_u = 0.07$
Distances (Å) (error ≈ 0.15 Å):
1Bi–1′Bi: 3.26[g] 1Bi–2Bi: 3.00 1Bi–2′Bi: 3.55 1Bi–4Bi: 3.29
2Bi–5Bi: 3.39 2Bi–4Bi: 3.06 3Bi–5Bi: 3.25 3Bi–3′Bi: 3.61[g] 3Bi–6′Bi: 3.25[g]
4Bi–5Bi: 3.31 4Bi–6Bi: 3.43 4Bi–7Bi: 3.48
5Bi–7Bi: 3.15 6Bi–8Bi: 3.42 7Bi–8Bi: 3.64 8Bi–9Bi: 3.18

[a]Displacements relative to ideal $(\sqrt{2} \times \sqrt{2})$ positions.
[b]Overall parameter for all atoms.
[c]Non-refined parameter.
[d]Parameter refined stepwise and kept constant during refinement of the others.
[e]Dependent parameter.
[f]Only one Cu atom of the layer listed.
[g]Distance to symmetry equivalent Bi (labeled by prime).

be 3.13 Å (average of the four independent values between the Bi atom pairs 1–2, 4–2, 4–5 and 7–5), whereas the separation parallel to the dislocation axis is reduced to 3.42 Å (average of five distances 2–5, 1–4, 4–7, 6–8, 3–3′), instead of 3.615 Å. In this context, we should emphasize that although the error bar of the distance determination for the p(10 × 10) structure is in the range of 0.15 Å, the average distances mentioned above are considerably more reliable due to their strong effect on the reflection intensities along the corresponding directions in reciprocal space. We estimate an error bar of about 0.05–0.10 Å for the average distances. Clearly, the extra degree of freedom in the two-dimensional array leads to a general contraction within the core of the dislocation. Whether the contraction arises because of tension within the one-dimensional wall or the packing requirements of the vertices (see below) cannot be determined. That the average diagonal distance is 5% smaller than the bulk Bi value is not a surprise, as interatomic contractions of bond lengths are generally found in the surface layers of metals due to the reduced coordination of surface atoms. The coordination of the Bi atom right in the vertex itself (designated #1 in Table 2) also appears to be fivefold. It has in-plane Bi neighbors at 3.26 Å (#1′), 3.00 Å (#2), 3.55 Å (#2′) and 3.29 Å (#4), averaging to 3.27 Å, which is about the same as the bulk Bi bond length of 3.29 Å. The ideal hollow sites are only 2.55 Å apart here, so there is a clear shift radially outwards, which is probably associated with the contraction along the domain walls mentioned above.

The remainder of the discussion of the p(10 × 10) structure concerns the atomic positions within the 3 × 4 rectangular islands themselves. The average Bi–Bi spacing within the islands is 3.43 Å, slightly contracted from the ideal 3.615 Å $(\sqrt{2} \times \sqrt{2})$ spacing. The average of the four Bi–Bi

distances between the domain walls and the islands is 3.44 Å, which is not significantly different. There is an apparent discrepancy with the corresponding 3.28 Å value for the $c(9\sqrt{2}\times\sqrt{2})$-structure, but this latter number should be averaged with the lateral 3.615 spacing because of the uniaxial strain; the resulting 3.45 Å then compares favorably.

In summary, the average distances within the square-coordinated $(\sqrt{2}\times\sqrt{2})$-like regions of both structures appear to contract to about 3.44 (10) Å, whereas the intervening surface dislocations have an average internal (diagonal) spacing in the $c(9\sqrt{2}\times\sqrt{2})$-structure of 3.38 (10) Å, compared with 3.13 (10) Å for the higher density $p(10\times10)$. Since this is the most significant difference between the two structures, it suggests that the place where misfit is most readily accommodated in a heavy domain wall is right inside the core itself. These are the atoms most displaced from hollow sites, and are apparently the most easily moved atoms to accommodate different domain-wall configurations.

Acknowledgements

The authors would like to thank J.J. Csiszar for maintenance of the rotating X-ray source and R. Wunderlich for preparing the figures. M. De Santis and I.K. Robinson acknowledge the hospitality of the SFB 338 during their visits in Munich.

References

[1] D.E. Moncton, P.W. Stephens, R.J. Birgenau, P.M. Horn, G.S. Brown, Phys. Rev. Lett. 46 (1981) 1533.
[2] P. Dimon, P.M. Horn, M. Sutton, R.J. Birgenau, D.E. Moncton, Phys. Rev. B 31 (1985) 437.
[3] H.L. Meyerheim, J. Wever, V. Jahns, W. Moritz, P.J. Eng, I.K. Robinson, Surf. Sci. 304 (1994) 267.
[4] F.C. Frank, J.H. van der Merve, Proc. R. Soc. Lond. Ser. A 198 (1949) 205.
[5] F.C. Frank, J.H. van der Merve, Proc. R. Soc. Lond. Ser. A 198 (1949) 216.
[6] F.C. Frank, J.H. van der Merve, Proc. R. Soc. Lond. Ser. A 198 (1949) 261.
[7] F.C. Frank, J.H. van der Merve, Proc. R. Soc. Lond. Ser. A 200 (1949) 125.
[8] V.L. Pokrowski, A.L. Talapov, Sov. Phys. JETP 51 (1980) 134.
[9] W. Hösler, W. Moritz, Surf. Sci. 175 (1986) 63.
[10] F. Bocquet, S. Gauthier, to be published.
[11] F. Delamare, G.E. Rhead, Surf. Sci. 35 (1972) 172.
[12] C. Argile, G.E. Rhead, Surf. Sci. 78 (1978) 115.
[13] H.L. Meyerheim, H. Zajonz, W. Moritz, I.K. Robinson, Surf. Sci. Lett. 381 (1997) L551.
[14] R. Feidenhans'l, Surf. Sci. Rep. 10 (1989) 105.
[15] I.K. Robinson, in: G.S. Brown, D.E. Moncton (Eds.), Handbook of Synchrotron Radiation, vol. 3, Elsevier, Amsterdam, 1991.
[16] R.W.G. Wyckoff, Crystal Structures, vol. 1, Interscience, New York, 1960.
[17] F. Jona, Surf. Sci. 8 (1967) 57.